Volume 62
Number 25
31 March 2026
Pages 6631–6818

ChemComm

Chemical Communications

rsc.li/chemcomm

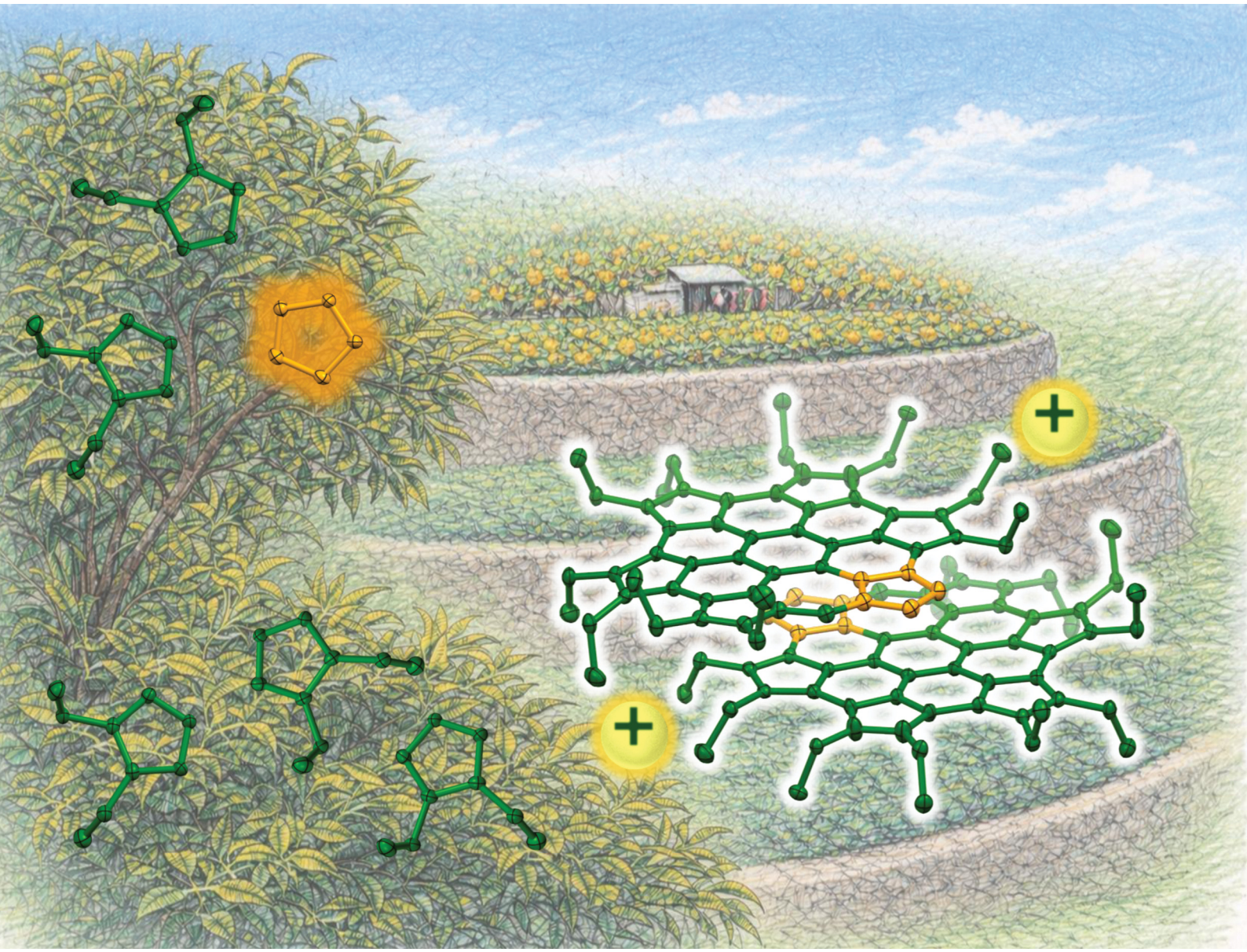

ISSN 1359-7345

ROYAL SOCIETY OF CHEMISTRY

COMMUNICATION

Masayoshi Takase *et al.*

π-Stacked dimerization of an antiaromatic homoHPHAC monocation

ChemComm

COMMUNICATION

View Article Online
View Journal | View Issue

Cite this: *Chem. Commun.*, 2026, **62**, 6716

Received 29th December 2025,
Accepted 3rd March 2026

DOI: 10.1039/d5cc07392h

rsc.li/chemcomm

π-Stacked dimerization of an antiaromatic homoHPHAC monocation

Kaito Wada,[a] Yuma Tanioka,[a] Shigeki Mori,[bc] Hidemitsu Uno[a] and Masayoshi Takase *[ac]

An antiaromatic homoHPHAC monocation unexpectedly forms a slipped π-stacked structure in solution and the solid state, representing a rare example of an antiaromatic π-dimer. In acetone-d_6 at 298 K, the association constant is 5.5 × 10^2 M^{-1} (ΔH = −22.0 kJ mol^{-1}, ΔS = −22.5 J K^{-1} mol^{-1}), with dimerization accompanied by attenuation of antiaromatic destabilization.

Planar aromatic molecules with 4n + 2 π electrons typically assemble through π–π stacking interactions; however, repulsion between filled π orbitals generally enforces an offset geometry rather than ideal face-to-face stacking.[1–6] In contrast, open-shell π-conjugated systems such as neutral radicals and radical cations can form face-to-face π-dimers, driven by favourable interactions between singly occupied molecular orbitals (SOMOs).[7–12] Beyond open-shell species, antiaromatic molecules possessing 4*n* π electrons have attracted increasing interest. Theoretical studies have predicted that face-to-face stacking of such molecules can alleviate intrinsic antiaromaticity through intermolecular orbital interactions, leading to so-called stacked aromaticity.[13–17] Nevertheless, antiaromatic molecules are generally expected to avoid planarity and close intermolecular contacts, instead alleviating their destabilization through symmetry-lowering distortions, bond-length alternation, or chemical transformations. As a result, the experimental realization of planar and stable antiaromatic systems capable of exhibiting stacked aromaticity remains highly challenging.

To date, norcorrole derivatives constitute one of the few experimentally validated examples that satisfy this concept (Fig. 1a).[18–21] Shinokubo and co-workers demonstrated that covalently linked norcorrole dimers, cyclophanes, and electron-deficient norcorroles exhibit pronounced reductions in antiaromaticity and distinct aromatic characteristics compared with their monomeric counterparts.[18–21] Despite these seminal studies, examples of stacked antiaromatic systems remain scarce, and the scope of molecular frameworks capable of such behaviour is still largely unexplored.

In our previous work, we reported antiaromatic π-extended HPHAC monocation, homoHPHAC **1**, which can be reversibly oxidized to an aromatic trication (Fig. 1b).[22,23] Notably, **1a** is stable even without *meso* substitution, in sharp contrast to norcorroles.[18,24–26] Although the phenyl-substituted analogue **1b** was structurally characterised by X-ray diffraction, steric congestion imposed by peripheral substituents induced a

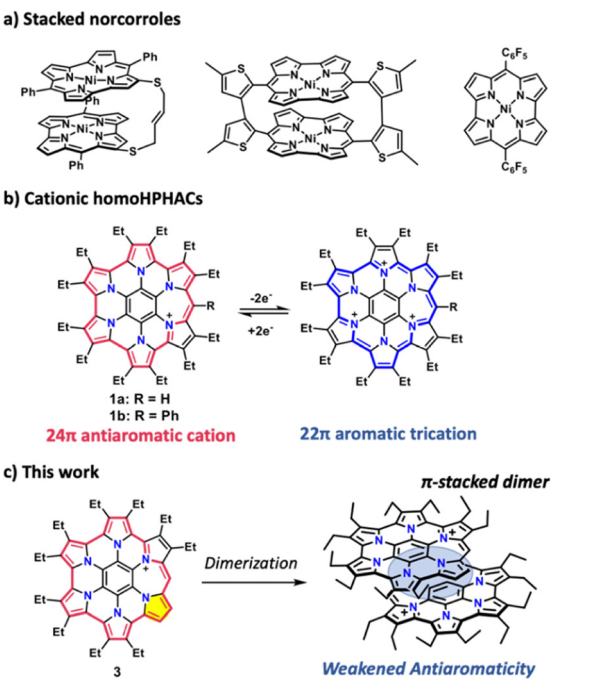

Fig. 1 (a) Chemical structures of stacked norcorroles, (b) previously reported cationic homoHPHACs **1a,b** and (c) π-stacked dimerization of antiaromatic homoHPHAC monocation **3** studied in this work.

[a] *Graduate School of Science and Engineering, Ehime University, Matsuyama 790-8577, Japan. E-mail: takase.masayoshi.ry@ehime-u.ac.jp*
[b] *Advanced Research Support Center (ADRES), Ehime University, Matsuyama 790-8577, Japan*
[c] *Research Unit on Molecular Materials Science for Toroidal π-Electron Systems, Ehime University, Matsuyama 790-8577, Japan*

curved geometry which, together with the influence of the peripheral ethyl groups, precluded effective intermolecular interactions. We therefore envisioned that reducing steric hindrance at the pyrrolic termini would enable controlled stacking[27,28] of closed-shell antiaromatic monocations, allowing stabilization through alleviation of antiaromaticity to overcome electrostatic repulsion. Herein, we report the synthesis and structural characterization of a *meso*- and the adjacent pyrrole-unsubstituted homoHPHAC monocation **3** (Fig. 1c) and demonstrate that it forms a π-stacked dimer in both solution and the solid state, accompanied by attenuation of its intrinsic antiaromatic destabilization.

Synthesis of homoHPHAC monocation **3** is shown in Scheme 1. DEHPB bearing a pyrrole unit without β-substitution was synthesized according to the reported procedure.[28] Treatment of DEHPB with 6.6 equivalents of DDQ at room temperature for 2 days afforded the partially cyclised product **2** (secoHPHAC). The structure of **2** was confirmed by ^{1}H NMR spectroscopy and high-resolution LDI–TOF mass spectrometry (see the SI). The preferential formation of secoHPHAC *via* selective cyclisation is presumably attributable to the facile generation of a radical cation intermediate during the Scholl reaction.[29] Subsequently, **2** was reacted with a Vilsmeier reagent prepared from DMF and $POCl_3$, following a procedure analogous to that reported previously.[22] After aqueous work-up with KPF_6, the desired homoHPHAC monocation **3** was obtained. Compound **3** is sufficiently stable to allow purification by alumina column chromatography, and its structure was determined by ^{1}H and ^{13}C NMR spectroscopy, high-resolution LDI–TOF mass spectrometry and single-crystal X-ray diffraction analysis.

Single crystals of **3** suitable for X-ray crystallographic analysis were obtained as the SbF_6^- salt by vapour diffusion using chloroform as a good solvent and toluene as a poor solvent. X-ray diffraction analysis revealed the absence of solvent molecules in the crystal lattice and confirmed that **3** exists as a *meso*-unsubstituted monocationic species (Fig. 2a and b). Owing to the absence of two ethyl substituents adjacent to the *meso* position, **3** adopts a highly planar structure, in contrast to the curved conformation observed for **1b**. Notably, analysis of the packing structure showed that, despite its monocationic nature, **3** forms a π-stacked dimer, with an average interplanar distance of 3.33 Å and a shortest intermolecular atom–atom distance of 3.28 Å (Fig. 2b and c). The stacking geometry corresponds to a slip-stacked arrangement in which the *meso* positions of the two molecules are oriented in opposite directions. In addition, CH–π interactions were identified between neighbouring dimers. It has been reported that in π-stacked dimers of norcorroles, which are intrinsically antiaromatic, the antiaromatic character of the monomer is attenuated and, in some cases, aromatic character emerges.[18–21] To evaluate the (anti)aromaticity of **3**, harmonic oscillator model of aromaticity (HOMA) values based on bond-length equalisation were calculated. For the macrocyclic conjugated framework highlighted by the thick red bonds in Fig. 1c and Scheme 1, a HOMA value of 0.74 was obtained for **3**, which is significantly higher than that of **1b** (0.67) and the optimised structure of the methyl-substituted analogue **3**-Me (0.70) (Fig. S8). A similar trend of bond-length equalization upon dimerization has been reported in previous studies on stacked norcorroles.

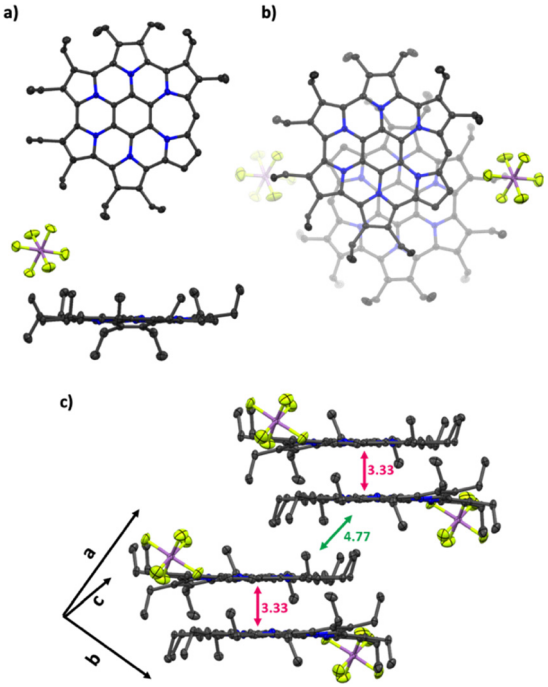

Fig. 2 Crystal structures of **3**. (a) Top and side views, (b) top view of π-stacked dimer and (c) packing structure. For clarity, the disordered components with minor occupancy are omitted.

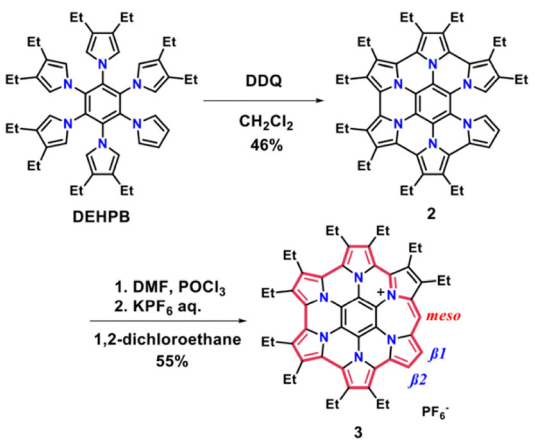

Scheme 1 Synthesis of secoHPHAC **2** and **3**.

To further elucidate the solution-state behaviour of **3** as the PF_6^- salt, concentration-dependent ^{1}H NMR measurements were performed (Fig. 3a and b). Upon increasing the concentration of **3** in acetone-d_6, pronounced downfield shifts were observed for the *meso* proton and the two pyrrolic β protons (0.69 mM → 5.19 mM; *meso*-H: δ = 3.92 → 4.24 ppm; β1-H: δ = 5.17 → 5.51 ppm; β2-H: δ = 4.88 → 5.42 ppm). In contrast, among the ethyl substituent signals, only the H1–H4 resonances exhibited comparable downfield shifts, whereas the remaining ethyl signals showed little or no change (Fig. S3b).

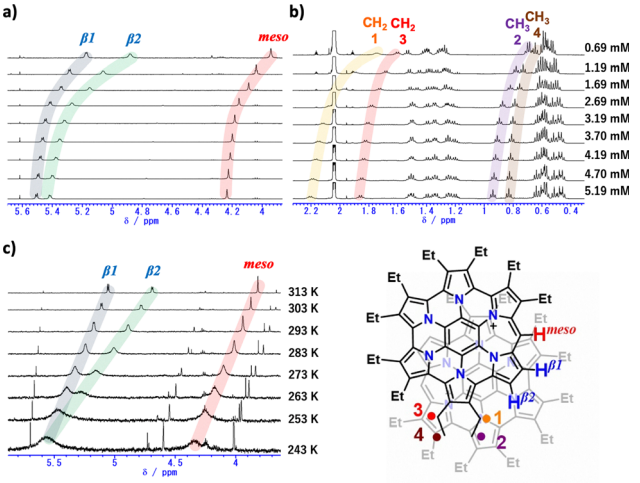

Fig. 3 (a) and (b) Concentration-dependent ^{1}H NMR spectra of **3** in acetone-d_6 at 298 K, shown in different spectral regions. Signal assignments were made on the basis of NOESY spectroscopy. (c) Temperature-dependent ^{1}H NMR spectra of **3** in acetone- d_6 ([**3**] = 0.69 mM), recorded between 243 and 313 K.

Such concentration-dependent behaviour was not observed for the previously reported **1a**; instead, only upfield signals were detected (*meso*-H: δ = 3.64 ppm; CH_2: δ = 1.42–1.60 and 1.69 ppm; CH_3: δ = 0.60–0.69 and 0.78 ppm).[22] In light of the single-crystal structural analysis of **3**, the *meso* and pyrrolic β protons and ethyl groups exhibiting downfield shifts are located above the π-surface of the opposing antiaromatic homoHPHAC framework. Collectively, these results indicate that, even in solution, slip-stacked dimers analogous to those observed in the solid state are formed under high-concentration conditions.

On the basis of the crystal structure and NMR analyses, homoHPHAC **3** was assumed to form a dimer in solution, and the association constant in acetone-d_6 at 298 K was determined by nonlinear regression analysis to be $(5.5 \pm 0.21) \times 10^2$ M^{-1} (ΔG_{298} = −15.6 kJ mol^{-1}), using the *meso*-proton signal for fitting (Fig. S4a). Notably, despite being a monocationic species, this value is comparable to the reported association constant of pentafluorophenyl-substituted norcorrole (6.0×10^2 M^{-1} in $CDCl_3$).[21] When evaluated in the more polar solvent DMSO-d_6, a slightly smaller value of $(4.8 \pm 0.24) \times 10^2$ M^{-1} (ΔG_{298} = −15.3 kJ mol^{-1}) was obtained (Fig. S3f and S4e). This solvent-dependent decrease in association strength is plausibly attributed to the high polarity of **3**, reflecting its monocationic nature. Subsequently, variable-temperature ^{1}H NMR measurements of **3** were performed (Fig. 3c; [**3**] = 0.69 mM). In acetone-d_6, decreasing the temperature resulted in pronounced downfield shifts of the *meso* proton and the two pyrrolic β protons. This behaviour indicates that the monomer–dimer association equilibrium observed in the concentration-dependent experiments is similarly modulated by temperature. To evaluate the thermodynamic parameters governing this equilibrium, association constants were determined at different temperatures (Table S4 and Fig. S4a–d). Analysis of these data using a van't Hoff plot afforded ΔH = −22.0 kJ mol^{-1} and ΔS = −22.5 J K^{-1} mol^{-1} (Fig. S5 and Table S5). The negative values of ΔH and ΔS indicate that dimer formation is enthalpically favourable but entropically unfavourable, consistent with general association processes. These results demonstrate that dimerization of **3** is strongly driven by enthalpic contributions.

To examine the concentration dependence of the oxidation potentials, cyclic voltammetry (CV) measurements of **3** were performed at different concentrations (Fig. S9). In dichloromethane, CV measurements at concentrations of 4.0 and 0.2 mM revealed first and second oxidation potentials of E^{ox1} = −0.08 V and E^{ox2} = 0.27 V (4.0 mM) and E^{ox1} = −0.10 V and E^{ox2} = 0.23 V (0.2 mM), respectively, indicating no discernible concentration dependence. These values are essentially identical to those reported for **1a** (E^{ox1} = −0.11 V and E^{ox2} = 0.21 V at 1.0 mM). This lack of concentration dependence is most likely due to the high concentration of supporting electrolyte present in solution ([$TBAPF_6$] = 100 mM). Notably, however, no appreciable concentration-dependent spectral changes were observed in the absorption spectra of **3** in both dichloromethane and acetone even in the absence of supporting electrolyte, including at higher concentrations up to 3.0 mM (Fig. S10b). The absorption spectra exhibit a broad and weak absorption band in the range of 1000–1750 nm, similar to that observed for **1b**, which is characteristic of antiaromatic molecules with narrow HOMO–LUMO gaps (Fig. S10a). These results suggest that, in contrast to ^{1}H NMR spectroscopy, absorption spectroscopy is insufficiently sensitive to detect the monomer–dimer equilibrium of **3** in solution under the present conditions.

In contrast, the solid-state absorption spectrum displays a distinct and broad absorption band in the shorter-wavelength region of 900–1500 nm (Fig. S10c). To gain insight into the origin of these spectral features, time-dependent density functional theory (TD–DFT) calculations were performed using monomeric and dimeric geometries extracted from the single-crystal structure. The calculated HOMO–LUMO transition for the monomer appears at 1574 nm with an oscillator strength (f) of 0.0277, whereas for the dimer this transition is hypsochromically shifted to 1461 nm and exhibits a markedly increased oscillator strength (f = 0.0681). These computational trends are in good agreement with the experimental absorption features observed in the solid state (Fig. S12b). Furthermore, molecular orbital energy analyses were carried out using DFT calculations. In the dimeric structure, the HOMO and HOMO−1, as well as the LUMO and LUMO−1, become quasi-degenerate, with both sets of orbitals stabilized relative to the corresponding orbitals of the monomer (Fig. S11c). Such stabilization of frontier molecular orbitals upon dimerization is a characteristic feature theoretically predicted for antiaromatic systems[13–17] and has been documented for stacked norcorroles and related π-dimeric architectures.[18–21] Consistent with these precedents, the present results suggest that intermolecular orbital interactions facilitate dimer formation of **3** and induce electronic reorganization, which contributes to attenuation of antiaromatic destabilization.

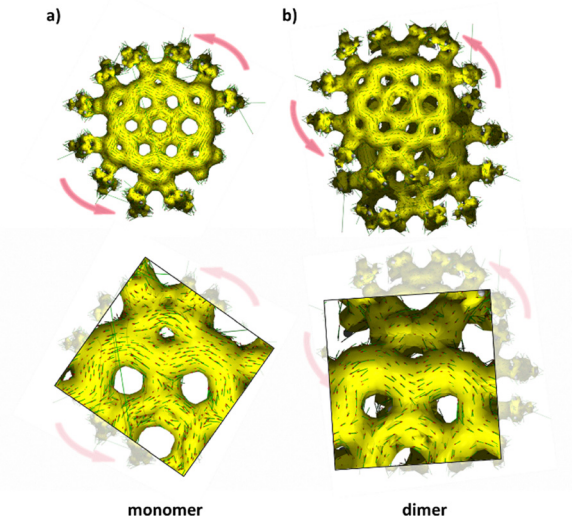

Fig. 4 ACID plots of **3**. (a) Monomer and (b) dimer (isovalue = 0.03). The magnetic field is applied perpendicular to the molecular plane and points out of the page. Red arrows indicate the paratropic (counterclockwise) ring current.

Finally, to gain insight into changes in antiaromatic character upon dimerization, nucleus-independent chemical shift (NICS)[30] and anisotropy and anisotropy of the induced current density (ACID)[31] calculations were performed. In the dimeric structure, small but discernible decreases in the NICS($\pm$ 1) values were observed at both the outside NICS(1) and the inside NICS($-$1) positions relative to those of the monomer, with a tendency toward a larger decrease at the inside position (Table S13). Consistent with these observations, comparison of the ACID plots reveals a modest reduction in the magnetic response upon dimerization (Fig. 4). In both the monomeric and dimeric forms, a counterclockwise paratropic ring current extending over the entire macrocyclic framework is observed, consistent with antiaromatic character; however, the density of the current vectors is lower in the dimer than in the monomer. Taken together, these results likely suggest that formation of even a slip-stacked π-stacked dimer is associated with partial attenuation of the intrinsic antiaromatic character of **3**.

In this study, we investigated the association behaviour and accompanying electronic structural changes of the antiaromatic homoHPHAC **3** in both solution and the solid state. Despite its cationic nature, **3** forms a slipped π-stacked dimer through π–π interactions, as evidenced by a bond-length equalization, stabilization of the frontier molecular orbitals, and small but discernible changes in magnetic aromaticity indices, including slightly reduced NICS values and a reduced paratropic current density in the ACID analysis. At present, however, the detailed mechanism by which dimerization leads to such electronic reorganization remains unclear. Further in-depth theoretical investigations will therefore be required to clarify the origin of these effects. Such studies are expected to provide deeper insight into the fundamental principles governing π-dimer formation and electronic modulation in antiaromatic systems.

Conflicts of interest

There are no conflicts to declare.

Data availability

All supporting data for this article are provided in the supplementary information (SI). Supplementary information is available. See DOI: https://doi.org/10.1039/d5cc07392h.

CCDC 2519098 contains the supplementary crystallographic data for this paper.[32]

Acknowledgements

This work was supported by JSPS KAKENHI (JP24K01470 (M. T.)). Y. T. acknowledges JSPS Research Fellowship for Young Scientists.

References

1 C. A. Hunter and J. K. M. Sanders, *J. Am. Chem. Soc.*, 1990, **112**, 5525.
2 R. Thakuria, N. K. Nath and B. K. Saha, *Cryst. Growth Des.*, 2019, **19**, 523.
3 E. M. Pérez and N. Martín, *Chem. Soc. Rev.*, 2015, **44**, 6425.
4 M. Iwane, T. Tada, T. Osuga, T. Murase, M. Fujita, T. Nishino, M. Kiguchi and S. Fujii, *Chem. Commun.*, 2018, **54**, 12443.
5 G. B. McGaughey, M. Gagné and A. K. Rappé, *J. Biol. Chem.*, 1998, **273**, 15458.
6 L. M. Salonen, M. Ellermann and F. Diederich, *Angew. Chem., Int. Ed.*, 2011, **50**, 4808.
7 K. Goto, T. Kubo, K. Yamamoto, K. Nakasuji, K. Sato, D. Shiomi, T. Takui, M. Kubota, T. Kobayashi, K. Yasui and J. Quyang, *J. Am. Chem. Soc.*, 1999, **121**, 1619.
8 S. Suzuki, Y. Morita, K. Fukui, K. Sato, D. Shiomi, T. Takui and K. Nakasuji, *J. Am. Chem. Soc.*, 2006, **128**(8), 2530.
9 Q. Xiang, J. Guo, J. Xu, S. Ding, Z. Li, G. Li, H. Phan, Y. Gui, Y. Dang, Z. Xu, Z. Gong, W. Hu, Z. Zeng, J. Wu and Z. Sun, *J. Am. Chem. Soc.*, 2020, **142**, 11022.
10 H. Yokoi, S. Hiroto and H. Shinokubo, *J. Am. Chem. Soc.*, 2018, **140**, 4649.
11 K. E. Preuss, *Polyhedron*, 2014, **79**, 1.
12 J. Joseph, M. Berville, J. Wytko, J. Weiss and H.-P. J. de Rouville, *Chem. – Eur. J.*, 2025, **31**, e202403115.
13 C. Corminboeuf, P. von, R. Schleyer and P. Warner, *Org. Lett.*, 2007, **9**, 3263.
14 D. E. Bean and P. W. Fowler, *Org. Lett.*, 2008, **10**, 5573.
15 J.-I. Aihara, *J. Phys. Chem. A*, 2009, **113**, 7945.
16 K. Okazawa, Y. Tsuji and K. Yoshizawa, *J. Phys. Chem. A*, 2023, **127**, 4780.
17 Y. Tsuji, K. Okazawa and K. Yoshizawa, *J. Org. Chem.*, 2023, **88**, 14887.
18 R. Nozawa, H. Tanaka, W.-Y. Cha, Y. Hong, I. Hisaki, S. Shimizu, J.-Y. Shin, T. Kowalczyk, S. Irle, D. Kim and H. Shinokubo, *Nat. Commun.*, 2016, **7**, 13620.
19 R. Nozawa, J. Kim, J. Oh, A. Lamping, Y. Wang, S. Shimizu, I. Hisaki, T. Kowalczyk, H. Fliegl, D. Kim and H. Shinokubo, *Nat. Commun.*, 2019, **10**, 3576.
20 H. Kawashima, S. Ukai, R. Nozawa, N. Fukui, G. Fitzsimmons, T. Kowalczyk, H. Fliegl and H. Shinokubo, *J. Am. Chem. Soc.*, 2021, **143**, 10676.
21 S. Kino, S. Ukai, N. Fukui, R. Haruki, R. Kumai, Q. Wang, S. Horike, Q. M. Phung, D. Sundholm and H. Shinokubo, *J. Am. Chem. Soc.*, 2024, **146**, 9311.
22 K. Oki, M. Takase, S. Mori and H. Uno, *J. Am. Chem. Soc.*, 2019, **141**, 16255.
23 M. Takase, T. Takata, K. Oki, S. Mori and H. Uno, *Chem. Sci.*, 2023, **14**, 7036.

24 T. Ito, Y. Hayashi, S. Shimizu, J.-Y. Shin, N. Kobayashi and H. Shinokubo, *Angew. Chem., Int. Ed.*, 2012, **51**, 8542.
25 T. Yoshida, D. Sakamaki, S. Seki and H. Shinokubo, *Chem. Commun.*, 2017, **53**, 1112.
26 S. Ukai, Y. H. Koo, N. Fukui, S. Seki and H. Shinokubo, *Dalton Trans.*, 2020, **49**, 14383.
27 M. Ikeda, Y. Sasaki, Y. Fujikawa, S. Mori, K. Konishi, K. Ohara, H. Dekura, H. Toyota, M. Takase, A. M. Shirai, Y. Murotani, R. Matsunaga and T. Naito, *J. Mater. Chem. C*, 2025, **13**, 12650.
28 Y. Sasaki, M. Takase, S. Mori and H. Uno, *Molecules*, 2020, **25**, 2486.
29 L. Zhai, R. Shukla, S. H. Wadumethrige and R. Rathore, *J. Org. Chem.*, 2010, **75**, 4748.
30 Z. Chen, C. S. Wannere, C. Corminboeuf, R. Puchta and P. V. R. Schleyer, *Chem. Rev.*, 2005, **105**, 3842.
31 D. Geuenich, K. Hess, F. Köhler and R. Herges, *Chem. Rev.*, 2005, **105**, 3758.
32 CCDC 2519098: Experimental Crystal Structure Determination, 2026, DOI: 10.5517/ccdc.csd.cc2qkb7w.

